HHS Public Access

Author manuscript

Dev Dyn. Author manuscript; available in PMC 2016 October 01.

Published in final edited form as:

Dev Dyn. 2015 October ; 244(10): 1313–1327. doi:10.1002/dvdy.24303.

Deficiency of the RNA binding protein Caprin2 causes lens defects and features of Peters anomaly

Soma Dash[1], **Christine A. Dang**[1], **David C. Beebe**[2], and **Salil A. Lachke**[1,3,*]

[1]Department of Biological Sciences, University of Delaware, Newark, DE 19716 USA

[2]Department of Ophthalmology and Visual Sciences, Washington University, St. Louis, MO 63110 USA

[3]Center for Bioinformatics & Computational Biology, University of Delaware, Newark, DE 19716 USA

Abstract

Background—It was recently demonstrated that deficiency of a conserved RNA binding protein (RBP) and RNA granule (RG) component Tdrd7 causes ocular defects including cataracts in human, mouse and chicken, indicating the importance of post-transcriptional regulation in eye development. Here we investigated the function of a second conserved RBP/RG component Caprin2 that is identified by the eye gene discovery tool *iSyTE*.

Results—*In situ* hybridization, western blotting and immunostaining confirmed highly enriched expression of Caprin2 mRNA and protein in mouse embryonic and postnatal lens. To gain insight into its function, lens-specific *Caprin2* conditional knockout (cKO) mouse mutants were generated using a lens-Cre deleter line *Pax6GFPCre*. Phenotypic analysis of $Caprin2^{cKO/cKO}$ mutants revealed distinct eye defects at variable penetrance. Wheat germ agglutinin staining and scanning electron microscopy demonstrated that $Caprin2^{cKO/cKO}$ mutants have an abnormally compact lens nucleus, which is the core of the lens comprised of centrally located terminally differentiated fiber cells. Additionally, $Caprin2^{cKO/cKO}$ mutants also exhibited at 8% penetrance a developmental defect that resembles a human condition called Peters anomaly, wherein the lens and the cornea remain attached by a persistent stalk.

Conclusions—These data suggest that a conserved RBP Caprin2 functions in distinct morphological events in mammalian eye development.

Keywords

Lenti-corneal stalk; Mouse development; Gene expression; Lens nucleus compaction; RNA granule component; *iSyTE*

[*]Corresponding author: Salil A. Lachke, Ph.D., Department of Biological Sciences, University of Delaware, Newark, DE 19716 USA, Tel.: (617) 959 9193, Fax: (302) 831 2281, salil@udel.edu.

Introduction

Eye development in mammals is initiated in late gastrulation and involves coordinated morphogenesis between the optic vesicle and the non-neural surface ectoderm resulting in the formation of the neural retina and the lens, respectively (Cvekl and Ashery-Padan, 2014; Donner et al., 2006; Lachke and Maas, 2010). During early stages of anterior eye chamber/segment (comprising of cornea, lens, iris, and ciliary body) development, cells of the lens placode invaginate together to form a lens pit that subsequently develops into a lens vesicle, while overlying cells that reconstitute the ectodermal surface contribute toward corneal epithelium tissue (Cvekl and Duncan, 2007). In later stages, cells of mesenchymal origin migrate to contribute to the corneal endothelium tissue (Cvekl and Tamm, 2004; Hay, 1980). During these critical developmental events controlled by an interplay of transcription factors and signaling molecules, cells of the surface ectoderm undergo substantial changes in their shape as well as in their adhesion properties (Hendrix and Zwaan, 1974; Lang et al., 2014; Plageman et al., 2011, 2010; Pontoriero et al., 2009, 2008). Indeed, perturbation of these complex processes leads to incomplete separation of the lens vesicle from the overlying corneal ectoderm in turn resulting in the presence of an abnormal lenti-corneal stalk, which is a feature associated with the human developmental defect called Peters anomaly (Bhandari et al., 2011; Reis and Semina, 2011).

In the normally formed lens vesicle, anteriorly localized cells contribute to the epithelium of the lens while posteriorly localized cells begin differentiation into primary fiber cells that elongate to fill up the lens vesicle and contribute to the “nucleus” of the lens (Cvekl and Duncan, 2007). Through development and adulthood, cells of the anterior lens epithelium remain in the cell cycle and undergo division in a specific region of the lens called the proliferation zone. Just beyond the proliferation zone near the equator of the lens, epithelial cells respond to signaling cues and exit the cell cycle to begin differentiation into secondary fiber cells (Lovicu and McAvoy, 2005). Fiber cells undergo a terminal differentiation program that results in high levels of expression of structural proteins such as crystallins as well as transport proteins such as aquaporins and gap junction proteins, followed by the loss of their nuclei and organelles (Bassnett et al., 2011; Cvekl and Duncan, 2007). Perturbations in fiber cell differentiation or homeostasis result in lens defects that include cataracts (Churchill and Graw, 2011; Shiels and Hejtmancik, 2013). Furthermore, morphological changes in the lens, such as compaction of the lens nucleus due to genetic perturbation or aging are also associated with cataract (Al-Ghoul et al., 2001; Fudge et al., 2011).

Thus, to understand the pathogenesis of these ocular defects, it is important to identify the regulatory molecules that function in the development of eye tissue. In addition to conserved transcription factors and signaling molecules, it was recently demonstrated that Tdrd7, an RNA binding protein (RBP) and RNA granule (RG) component functions in vertebrate lens development (Lachke et al., 2011). This finding has initiated the investigation of other post-transcriptional regulatory molecules in eye development (Lachke and Maas, 2011). Here, we used a systems approach termed *iSyTE* (*i*ntegrated *Sy*stems *T*ool for *E*ye gene discovery) that has previously led to identification and characterization of several important genes that function in the lens (Agrawal et al., 2015; Kasaikina et al., 2011; Lachke et al., 2012a, 2012b, 2011; Manthey et al., 2014a, 2014b; Terrell et al., 2015; Wolf et al., 2013) to identify

a second RBP/RG component Caprin2 (Cytoplasmic activation- and proliferation-associated protein 2; also known as RNA granule protein 140, RNG140; C1q Domain-containing protein 1, C1qdc1; EEG1) as a candidate that likely functions in lens development. Caprin family proteins are conserved among metazoans, and human CAPRIN2 protein shares 51% identity and 73% similarity with Drosophila CAPR across a conserved region termed Homology Region 1 (Papoulas et al., 2010). Caprin2 has multiple conserved domains including the coiled-coil and the RGG domains, and the C1q domain found in the TNF protein super-family, which facilitate protein-RNA and protein-protein interactions, respectively (Shiina and Tokunaga, 2010). Interestingly, Caprin2 has recently been independently recognized as a gene responsive to induction by FGF8 in chicken lens fiber cells (Lorén et al., 2009), supporting the hypothesis for its potential function in the lens. Here, we characterized Caprin2 expression in mouse lens development and investigated its function by generating lens-specific *Caprin2* deletion mouse mutants. We find that *Caprin2* deficiency results in two distinct ocular defects at variable penetrance, one affecting the lens fiber cell core and the other impairing the separation of the lens and cornea tissue.

Results

Expression of Caprin2 in the Mouse Lens

The *iSyTE* approach analyzes microarray expression profiling datasets for wild type mouse lens at different stages of development. Importantly, it is based on a strategy termed "*in silico* subtraction" which effectively removes highly expressed but non-lens specific housekeeping genes, in turn, allowing identification of candidates with high lens-enriched expression – regardless of their absolute expression. In past, *iSyTE*-based lens-enrichment scores have proved to be reliable predictors of gene function in the lens and have been linked to lens defects (Lachke et al., 2012). Therefore we used *iSyTE* to identify the RBP/RG gene *Caprin2* as a highly lens enriched candidate with potential function in eye biology (Fig. 1A). Analysis of *iSyTE* tracks for lens embryonic stages indicated that *Caprin2* is expressed in the lens beginning from E10.5, and identified it to be among the top 1% of lens-enriched genes at E12.5 (Fig. 1A). To extend *Caprin2* expression beyond the three embryonic stages in the current version of *iSyTE*, we analyzed publicly available mouse lens microarray datasets at developmental stages between E16.5, E17.5, P0, P2, and P56. Together these analyses indicated that *Caprin2* exhibits significant lens-enriched expression in all stages tested (Fig. 1B). Further, *Caprin2* expression progressively increased in lens development with highest expression at P0 prior to being reduced at P56. Interestingly, western blot analysis demonstrated that Caprin2 protein is highly expressed in early postnatal stages, as expected from the microarray data, but its expression is down-regulated to undetectable levels at age 4.5 months (stage P135) (Fig. 1C).

To further investigate its expression within the lens, we next performed *in situ* hybridization at E12.5 and E14.5 and detected *Caprin2* transcripts specifically in fiber cells (Fig. 1D, E). Moreover, this analysis indicated *Caprin2* expression to be highly lens-enriched compared to other regions of the embryonic head tissue (Fig. 1F), partially explaining its high enrichment score in *iSyTE*. Immunostaining of mouse E13.5, E15.5, and E19.5 head tissue with a Caprin2-specific antibody corroborated this data, demonstrating that Caprin2 protein

expression is restricted to lens fiber cells, while being undetected in lens epithelial cells (Fig 1G–I). Further, this analysis revealed that Caprin2 protein localizes predominantly in the cytoplasm of fiber cells. Together, these analyses support *iSyTE*'s prediction of high Caprin2 expression in the lens.

Generation of *Caprin2$^{cKO/cKO}$* Lens-Knockout Mice

Caprin2$^{cKO/cKO}$ conditional knockout mouse mutants were generated by deleting in lens lineage cells the fifth exon of *Caprin2*, which codes for a basic helix domain involved in RNA binding (see Experimental Procedures for details) (Fig. 2A). This was achieved by crossing mice carrying *Caprin2* conditional null alleles (*Caprin2* exon 5 flanked by *loxP* sites; *Caprin2^{flox}*) with *Pax6GFPCre* mice, in which beginning at E8.75 Cre recombinase expression is driven by the *Pax6* ectodermal enhancer and P0 promoter in surface ectodermal cells fated to become lens (Rowan et al., 2010, 2008). Deletion of *Caprin2* exon 5 is expected to lead to *de novo* splicing of exon 4 and exon 6, causing a frame-shift in the *Caprin2* open reading frame (ORF) and resulting in a downstream pre-mature stop codon (Fig. 2A). This in turn is expected to lead to nonsense-mediated decay of the truncated *Caprin2* transcript expressed from the recombined allele in cells fated to become the lens. These expected results were confirmed by reverse transcriptase PCR (RT-PCR), which demonstrated that *Caprin2* transcripts were undetected in *Caprin2$^{cKO/cKO}$* lenses (Fig. 2B). Further, western blot analysis confirmed that Caprin2 protein expression is undetected in *Caprin2$^{cKO/cKO}$* lenses at P56 (Fig. 2C). Finally, immunostaining demonstrated that Caprin2 protein is severely reduced but present at detectable levels in *Caprin2$^{cKO/cKO}$* lens at E12.5 (Fig. 2D, E), but is undetected in the mutant lenses by stage P4 (Fig. 2F, G). These analyses indicate that genetic deletion of *Caprin2* exon 5 that leads to the absence of Caprin2 transcripts and protein was achieved in the lenses of *Caprin2$^{cKO/cKO}$* mutant mice.

Caprin2$^{cKO/cKO}$ Lens-Knockout Mice Exhibit Lens Defects

To investigate whether *Caprin2* deletion causes ocular defects in mice, we initiated the phenotypic characterization of *Caprin2$^{cKO/cKO}$* mutants. Lenses from mutant and control (*Pax6GFPCre:Caprin2$^{+/cKO}$*) animals were imaged by bright field microscopy at various stages. Although no lens opacities or overt cataracts were detected in majority of the *Caprin2$^{cKO/cKO}$* lenses (n=108), subtle differences near the putative cortical-nuclear boundary could be discerned in these mutant lenses (Fig. 3A, B) at high penetrance (60%) at age 2 months (P60) (Table 1). Specifically, while a ring-like demarcation between the cortical and nuclear fiber cells is apparent in control lenses (Fig. 3A), it is absent in majority of *Caprin2$^{cKO/cKO}$* mutant lenses (Fig. 3B). To characterize this defect further, we performed histological analysis on *Caprin2$^{cKO/cKO}$* mutant and control lenses at 1 month (P30). This analysis revealed no obvious fiber cell or nuclear degradation defects in mutant lenses (Fig. 3C, D).

Therefore, to investigate the nature of this abnormality at high resolution, we performed scanning electron microscopy (SEM) on control and mutant lenses at age 1 month (P30) (Fig. 3E, F). SEM analysis demonstrated that deep into the lens tissue, nuclear fibers were observed in controls as expected (Fig. 3G). However, at comparable depths into the lens, in place of nuclear fibers *Caprin2$^{cKO/cKO}$* mutant lenses exhibited cortical fiber cell

morphology (Fig. 3H). This suggests that the region that forms the lens nucleus is potentially reduced in *Caprin2*$^{cKO/cKO}$ mutants. To test this possibility, we subjected mutant and control lenses at P0 with wheat germ agglutinin (WGA) staining. WGA is a lectin that preferentially binds to sialic acid and *N*-acetyl-*D*-glucosaminyl residues on cell membranes and preferentially stains the ball and socket regions of secondary fiber cells (now referred as membrane protrusions in the lens literature; while other structures in cortical fiber regions are termed as ball and sockets) (Kistler et al., 1986). Hence WGA differentially marks the lens cortex region (which stains at higher intensity) compared to the lens nucleus region (which stains at lower intensity). We measured the area of nuclear fibers (lower WGA staining intensity) compared to the total area of the lens in control and mutants. This analysis indicates that as expected from bright field imaging and SEM data, *Caprin2*$^{cKO/cKO}$ mutant lenses exhibit a significantly reduced area of lens nucleus compared to controls (Fig. 4A–C). Together, these data suggest that *Caprin2*$^{cKO/cKO}$ mutants exhibit fiber cell nuclear compaction defects. To investigate potential actin-based cytoskeletal defects underlying this phenotype, we examined the F-actin deposition pattern by staining whole lens as well as lens sections of control and *Caprin2*$^{cKO/cKO}$ mutants by the bicyclic peptide, phalloidin. This analysis demonstrated that F-actin deposition is unaltered in *Caprin2*$^{cKO/cKO}$ mutant lenses suggesting that fiber cell architecture is maintained in these lenses (Fig. 4D–G).

Caprin2$^{cKO/cKO}$ Lens-Knockout Mice Exhibit Features of Peters Anomaly

Of the 108 *Caprin2*$^{cKO/cKO}$ mutant eyes analyzed, 8% exhibited corneal and lens opacities at variable intensities (Fig. 5A) (Table 1). This subset of mutant eyes also exhibited a persistent lenti-corneal stalk (Fig. 5B), which is commonly observed in the human developmental defect Peters anomaly. Except in the case of one mutant that exhibited this defect in both eyes, eight other *Caprin2*$^{cKO/cKO}$ mutants exhibited the lenti-corneal stalk in a unilateral manner. None of the *Pax6GFPCre:Caprin2*$^{+/cKO}$ control eyes exhibited this defect (n=121). This phenotype suggested that Caprin2 may potentially also function in an early phase in eye development, perhaps in lens vesicle closure. To gain insight into how Caprin2 deficiency may cause an abnormal lenti-corneal stalk, we investigated Caprin2 expression in early eye development by immunostaining E10.5 wild type mouse lenses with Caprin2-specific antibody. This analysis demonstrated that Caprin2 protein is expressed in the lens at this stage (Fig. 5C). To aid visualization of the E10.5 lens morphology, we performed immunostaining with Jag1, which is highly expressed in the cytoplasm of E10.5 lens pit cells (Fig. 5C′) (Le et al., 2012). Notably, Caprin2 exhibits higher expression in cells located in the anterior region of the lens pit near the “rim” (Fig. 5D–F). Interestingly, at higher magnification, Caprin2 staining in these cells appeared granular (Fig. 5E, F). This expression analysis indicates that at E10.5, Caprin2 is detected specifically in cells that likely undergo dynamic changes during separation of the lens vesicle from the surface ectoderm. Thus, in addition to its function in lens fiber cells, Caprin2 may function in an early phase of eye development, as indicated by its perhaps efficient early deletion in a subset of mutants, which causes a persistent lenti-corneal stalk.

WGA Staining of *Caprin2*$^{cKO/cKO}$ Embryonic Lenses Suggests Fiber Cell Membrane Abnormalities

Because WGA staining differed between control and *Caprin2*$^{cKO/cKO}$ mutant lenses at age 1 month, we next investigated the WGA staining pattern in these animals at embryonic stages. Interestingly, *Caprin2*$^{cKO/cKO}$ mutant lenses exhibit higher intensity of WGA staining compared to control lenses at mouse embryonic stages E12.5, E14.5 and E16.5 (Fig. 6A–C′), further supporting the hypothesis that fiber cell membrane composition likely differs between these animals. To gain insights into the molecular basis of the lens defects in *Caprin2*$^{cKO/cKO}$ mice, we performed analysis of various lens epithelial and fiber cell marker genes. Specifically, *Caprin2*$^{cKO/cKO}$ mutant and control lenses were immunostained with Pax6, Foxe3, gamma Crystallin (Cryg), and Aquaporin 0 (Aqp0) proteins. While Pax6 and Foxe3 are transcription factors expressed in the lens epithelium, Cryg and Aqp0 are markers of lens fiber cells. There is no significant difference in the staining pattern of Pax6 (Fig. 6D–F′) and Foxe3 (Fig. 6G–I′) between control and mutant lenses. No significant difference was observed in Cryg (Fig. 7A–E′) and Aqp0 (Fig. 7F–J′) expression between control and *Caprin2*$^{cKO/cKO}$ mutant lenses even at postnatal stages. Further, we also investigated N-cadherin (N-cad), which is a component of cell-cell junctions in the lens. No significant staining pattern difference for N-cad was detected between control and mutant lenses (Fig. 7K–O′). These data indicate that while there are no overt defects in epithelium, fiber or cell adhesion marker genes in *Caprin2*$^{cKO/cKO}$ mutant lenses, they exhibit abnormalities in fiber cell membrane composition that are evident in embryonic stages.

The *Caprin2* paralog *Caprin1* is expressed in *Caprin2*$^{cKO/cKO}$ lenses

Because *Caprin2*$^{cKO/cKO}$ mutant lenses exhibit variable phenotypes that are not penetrant, we investigated expression of other Caprin family proteins in the lens that may cause potential redundancy. The *Caprin2* paralog *Caprin1* encodes an RNA granule protein and contains RGG boxes as well as basic helix domains, similar to Caprin2 (Shiina and Tokunaga, 2010; Solomon et al., 2007). Analysis of *Caprin1* in *iSyTE* indicates that it is not lens-enriched (Fig. 8A), but analysis of its absolute expression in lens microarray datasets at various embryonic and postnatal developmental stages indicated its high expression in the lens (Fig. 8B). Similar to *iSyTE*'s prediction, comparison of *Caprin1* expression in these lens datasets with WB microarrays provides further support that it is not lens enriched (Fig. 8C). We next investigated Caprin1 protein expression in *Caprin2*$^{cKO/cKO}$ mouse lenses and observed no significant difference in the expression levels of RNA (Fig. 8D) or protein in these mutants (Fig. 8E). Because defects in early lens developmental gene expression result in an abnormal lenti-corneal stalk, we examined Caprin1 protein expression at E10.5 by immunostaining and observed that it is cytoplasmic, and overlaps with the Caprin2 expression pattern in cells located at the rim of the lens pit (Fig. 8F–H). Further, immunostaining also indicates no change in Caprin1 protein localization within the lens in *Caprin2*$^{cKO/cKO}$ mutant lenses (Fig. 8I–N). These analyses demonstrate that although Caprin1 is highly expressed early in the lens at stages E10.5 and E12.5, it is progressively down-regulated in development and becomes restricted to the lens epithelium and cells of the transition zone (Fig. 8I, K, M). Together, these data indicate that the high expression and overlapping pattern of Caprin1 with Caprin2 during early embryonic stages might

compensate for the absence of Caprin2, and that *Caprin2* deletion does not alter the expression of Caprin1 in mouse lens. These findings, along with the residual presence of Caprin2 protein in early stages of *Caprin2*$^{cKO/cKO}$ mutant lenses, serve to explain the low penetrance of the Peters anomaly phenotype.

Discussion

In this study, we have applied *iSyTE* to identify a second RNA binding protein and RNA granule component Caprin2 to be highly enriched in the lens. Interestingly, *Caprin2* was first isolated as *EEG-1* from human bone marrow and erythroid progenitor cells (Aerbajinai et al., 2004), where it was associated with terminal differentiation of erythroblasts from a proliferative state into cells devoid of nuclei, analogous to the transition of lens epithelial cells into terminally differentiated fiber cells.

In the present study, our findings that Caprin2 exhibits highly enriched expression in mouse fiber cells beyond the lens pit stage is in agreement with a previous report that analyzed its expression in chicken and mouse lenses (Lorén et al., 2009). However, in the previous study Caprin2 protein expression was not detected in the lens prior to stage E11.5 (Lorén et al., 2009), while our current analysis demonstrates that Caprin2 protein exhibits a unique expression pattern at stage E10.5, being localized to granules that are around 0.7 μm in diameter, specifically in cells located at the anterior rim of the lens pit. The difference in these findings may be due to the use of different Caprin2-specific antibodies in these studies. Interestingly, both studies demonstrate that as lens development progresses, Caprin2 expression is restricted to fiber cells and is undetected in the anterior epithelium. This staining pattern – from being initially restricted to cells of the apical rim of lens pit to highly enriched expression in fiber cells – suggests that Caprin2 may have distinct functions in different stages of lens development.

Distinct Ocular Defects in *Caprin2* Mutants

To investigate its function in lens development, we generated conditional knockout *Caprin2*$^{cKO/cKO}$ mice and characterized these mutants to uncover two distinct ocular defects at variable penetrance: 1) a reduced lens nucleus region, and 2) presence of lenti-corneal stalk.

We find that at embryonic stages, *Caprin2*$^{cKO/cKO}$ lenses stain with WGA at higher intensity compared to control. Interestingly, higher intensity WGA staining of fiber cells is observed in cataractous lenses, albeit in aged lenses (Kistler et al., 1986). As WGA is known to recognize sugar moieties on membranes, the above result is suggestive of an alteration in membrane composition in *Caprin2*$^{cKO/cKO}$ embryonic lens fiber cells. Moreover, WGA is described to stain “ball and socket” junctions (referred to as “membrane protrusions” in recent reports), which are features of cortical fiber cells (Bassnett et al., 2011; Kistler et al., 1986; Scheiblin et al., 2014). Thus, these findings also suggest a pre-mature cortical-fiber cell characteristic that is acquired during embryonic development by these cells, which contribute to the lens nucleus in later stages. Nevertheless, these data suggest that although fiber cell differentiation appears to be unperturbed in *Caprin2*$^{cKO/cKO}$ lenses as suggested by normal staining of gamma Crystallins, Aquaporin 0 and N-cadherin, these mutant lenses

exhibit an alteration in fiber cell membrane composition, indicating that Caprin2 is important for acquiring the full characteristics of fiber cells. This alteration in fiber cell biology likely contributes to a reduction in the size of the lens nucleus, which is detected by both WGA staining and SEM analyses in post-natal stages in *Caprin2*$^{cKO/cKO}$ mutants.

Reduction in the lens nucleus, termed as “nuclear compaction”, occurs in human lenses as a process of aging (Augusteyn, 2010) and is associated with human age-related lamellar cataracts as well as to the loss of accommodative capability (Al-Ghoul et al., 2001; al-Ghoul and Costello, 1996, 1996; Augusteyn, 2010; Costello et al., 2013; Dubbelman et al., 2003; Michael and Bron, 2011). However, *Caprin2*$^{cKO/cKO}$ mutants do not exhibit cataracts even at age 6 months. Interestingly, a similar reduction of the lens nucleus is observed in *Bfsp2 (CP49)* knockout lenses (Fudge et al., 2011). However, the lens nucleus reduction in *Bfsp2 (CP49)* knockout lenses and *Caprin2*$^{cKO/cKO}$ mutant lenses may have different underlying molecular mechanisms of pathogenesis. This is because while the fiber cell ultrastructure is severely disrupted in *Bfsp2 (CP49)* knockout lenses (Fudge et al., 2011), histology and SEM analyses demonstrates that the fiber cell ultrastructure appears normal in *Caprin2*$^{cKO/cKO}$ lenses. These analyses were performed on animals in which the naturally occurring *Bfsp2 (CP49)* mutation contributed by the FVB/N background was confirmed to be absent (see Experimental Procedures for details), and we further validated by RT-PCR that *Bfsp2 (CP49)* expression was unaltered in control and mutant lenses (data not shown). It will be intriguing to investigate the full implication of the reduced lens nucleus defect and its underlying molecular pathogenic mechanism in *Caprin2*$^{cKO/cKO}$ lenses in future studies.

In addition to the above phenotype, a subset of *Caprin2*$^{cKO/cKO}$ mutants exhibit a lenti-corneal stalk, which is observed in a human ocular developmental defect termed Peters anomaly (Bhandari et al., 2011; Reis and Semina, 2011). Mutations or functional compromise in several genes have been linked to Peters anomaly in humans and mice. These are *B3GLCT* (*B3GALTL*), *Cdh1* and *Cdh2* (*E*- and *N-Cadherin*), *Cdo*, *Cited2*, *COL4A1*, *CYP1B1*, *Fgfr*, *FLNA*, *FOXC1*, *FOXE3*, *HCCS*, *Msx2*, *c-Myc*, *NDP*, *PAX6*, *PITX2*, *PITX3*, *Pxdn*, *RIEG1*, *Shroom3*, *SLC4A11*, *Sox11*, *Spry1*, *Spry2*, *TFAP2A* (*AP2α*), *Zeb2* (*Sip1*) (Bhandari et al., 2011; Cavalheiro et al., 2014; Chen et al., 2008; Kuracha et al., 2011; Lang et al., 2014; Okajima et al., 1999; Ozeki et al., 2001; Pontoriero et al., 2009, 2008; Reis and Semina, 2011; Weh et al., 2014; Wurm et al., 2008; Yan et al., 2014; Zhang et al., 2009; Zhao et al., 2012). It is interesting to note that Caprin2 protein is expressed in cells located at the anterior rim region of the lens pit at E10.5. During the process of lens vesicle separation, these opposing cells of the anterior rim of the lens pit have to come close together and form adherens junctions with each other. Thus, this process involves the dissolution of existing contacts with old cell neighbors and the initiation of new contacts with prospective cell neighbors. It can be speculated that recruitment of Caprin2 in these cells may be reflective of its function in facilitating lens vesicle closure and separation, and therefore absence of Caprin2 results in a persistent lenti-corneal stalk. This is discussed further in the following section.

Caprin2, Granules, and Signaling: A Speculation

Previously, Fgf signaling has been shown to induce Caprin2 expression in chicken lens explant tissue culture (Lorén et al., 2009). Thus it is possible that Fgf signaling may be involved in modulating Caprin2 function in early and/or later phases of mouse lens development. Studies on *Fgfr1* and *Fgfr2* conditional double knockout mouse mutants suggest that signaling through these receptors is required for lens placode cell survival, and no lens tissue is detected at stage E12.5 (Garcia et al., 2011). Further, expression of dominant negative Fgfr1IIIc in transgenic mice causes down-regulation of Peters anomaly-associated genes *Pax6* and *Foxe3* and results in a lenti-corneal stalk, thus suggesting a function for Fgf signaling in this phase of lens development (Faber et al., 2001). Interestingly, downstream targets of Fgfr signaling *Spry1* and *Spry2*, which are involved in its negative feedback regulation, when deleted in mice individually or together, lead to formation of a lenti-corneal stalk (Kuracha et al., 2011). Spry1 and 2 negatively modulate Fgfr signaling by antagonizing other Fgfr downstream targets, such as Ras-Raf-ERK (Hanafusa et al., 2002). Interestingly, *Spry1* and *Spry2* conditional double knockout mice exhibit ectopic expression of pERK and p63 in cells of the anterior margins of the lens pit, which are likely the same cells in which Caprin2 granules are enriched.

These findings indicate that in the early phase of lens development, deletion of three targets of Fgfr signaling, Spry1, Spry2 (Kuracha et al., 2011) and Caprin2 result in a lenti-corneal stalk. Thus, future studies can be aimed toward addressing the function of Caprin2 granules in these early events in lens development. Previously, Caprin granules have been implicated in post-transcriptional regulation by inhibition of protein translation from specific transcripts, a function that is conserved in Drosophila and human (Papoulas et al., 2010; Shiina and Tokunaga, 2010). It can be speculated that Caprin2 is involved in localized control of expression of specific proteins in the anterior rim of the lens pit. It will be interesting to test expression of markers such as pERK and p63 in *Caprin2* knockout mutants that exhibit a lenti-corneal stalk, and conversely testing *Caprin2* expression in *Spry1* and *Spry2* mutant lenses in future studies.

Low Penetrance of the Lens-Cornea Stalk Phenotype

A probable explanation for the low penetrance of the lenti-corneal stalk phenotype in $Caprin2^{cKO/cKO}$ mutants is due to the presence of the *Caprin2* paralog *Caprin1* in the lens. Our analysis shows that Caprin1 has overlapping expression with Caprin2 in early lens development, and therefore may compensate for the loss of Caprin2. This may be compounded by the presence of residual Caprin2 protein in early $Caprin2^{cKO/cKO}$ mutant lenses, further contributing to the low penetrance of the phenotype.

Conclusion

In summary, these findings provide new insights into the function of a second RNA binding protein/RNA granule component in mammalian eye development by demonstrating that *Caprin2* deficiency causes distinct defects such as reduction in the size of the lens nucleus and presence of a stalk between the lens and the cornea. Finally, besides *Bfsp2*, *Caprin2* is

identified here as a second candidate gene implied in nuclear compaction in the mammalian lens.

Experimental Procedures

Gene Expression Analysis using *iSyTE*

The *iSyTE* database (Lachke et al., 2012b) was analyzed for candidate genes that exhibited highly enriched expression in the lens. Among a genome-wide analysis, *Caprin2*, located on mouse chromosome 6, was identified to be among the top 1% of lens-enriched genes according to *iSyTE*. Further, to extend this analysis to other stages in lens, publically available lens Affymetrix microarray datasets were analyzed for *Caprin2*-specific probe-binding intensity. This analysis was performed for lens samples at stages E10.5, E11.5, E12.5, E16.5, E17.5, P0, P2, and P56 for which datasets were available at GEO. An extensive meta-analysis of these lens microarray datasets will be described in greater detail elsewhere (Atul Kakrana, Salil Lachke, manuscript in preparation). *Caprin2*-specific probe signal intensity was compared between each of the above lens samples and WB, and plotted as fold-change to provide an estimate of "enriched" expression in the lens.

Animals

Mice used in this study were housed in the animal facility at the University of Delaware. The Institutional Animal Care and Use Committee (IACUC) at the University of Delaware approved animal experimental protocols and all animal experiments were conducted in accordance with the Association of Research in Vision and Ophthalmology (ARVO) statement for the use of animals in ophthalmic and vision research. *Caprin2*$^{tm2a(EUCOMM)Wtsi}$ allele (henceforth referred to as *Caprin2*^{flox}) carrying mice generated by the Welcome Trust Sanger Institute were obtained from the European Mouse Mutant Archive (EMMA) (EMMA ID, EM:05381). Full description of the construct and deletion strategy is available at www.infrafrontier.eu and http://www.informatics.jax.org/allele/MGI:4434168. Briefly, a L1L2_gt0 cassette carrying *lacZ/neomycin* ORFs flanked by *FRT* sites and followed by a *loxP* site was first inserted upstream of *Caprin2* exon 5 and subsequently a second *loxP* site was inserted downstream of exon 5. Thus, Cre-based recombination activity is expected to remove *Caprin2* exon 5.

To generate *Caprin2* conditional knockout (*cKO*) mice, we used the *Pax6GFPCre* mouse line established by Drs. Sheldon Rowan and Richard Maas that expresses Cre recombinase driven by the activity of a conserved *Pax6* ectodermal enhancer with P0 promoter starting at E8.75 in the presumptive lens ectoderm (Rowan et al., 2010, 2008). Crosses between *Caprin2*^{flox} mutant allele carrying mice and *Pax6GFPCre:Caprin2*^{flox} mice led to generation of *Pax6GFPCre:Caprin2*$^{flox/flox}$ mice in which Caprin2 was deleted in lens cells (henceforth referred to as *Caprin2*$^{cKO/cKO}$). This is because excision of *Caprin2* exon 5 leads to the splicing of exon 4 and 6 in the resulting *Caprin2* transcripts. This leads to a frame-shift in the *Caprin2* ORF, which is subjected to nonsense-mediated decay of the transcript. These animals were maintained on a mixed background of C57BL/6J and FVB/N strains. The *Pax6GFPCre* line was always maintained on a *Cre* heterozygous background and was never found to exhibit any ocular defects in our analysis of these animals over a

period of 6 months. Because the mice had contributions from the FVB/N strain that carries the *Bfsp2 (CP49)* mutation, we performed genotyping for *Bfsp2 (CP49)* mutation as described (Simirskii et al., 2006) and no correlation was observed between the presence/absence of *Bfsp2 (CP49)* mutant allele and the ocular phenotypes in *Caprin2* mutant animals. All animals used for generating data shown in the figures were confirmed to have no *Bfsp2 (CP49)* mutant alleles. Genotyping was performed on DNA isolated from mouse tails and primers used in PCR were as follows: for wild-type allele, 5′ GCCTACCTTTCTGTGCCTCC 3′ and 5′ CCAGGCTACTCTCCCCAAAG 3′; for *Caprin2* mutant allele 5′ GCCTACCTTTCTGTGCCTCC 3′ and 5′ TCGTGGTATCGTTATGCGCC 3′; for *Cre* allele, 5′ TTCAATTTACTGACCGTACACC 3′ and 5′ CCGACGATGAAGCATGTTTAG 3′. *Caprin2*$^{cKO/cKO}$ mutant mice were physically evaluated for the presence of lens defects and cataracts, euthanized, and processed as required in experiments.

Bright Field Microscopy and Histology

Mouse eye tissue were dissected from euthanized control (*Pax6GFPCre:Caprin2*$^{+/cKO}$) and *Caprin2* $^{cKO/cKO}$ mutant animals and carefully cleaned in 1x phosphate buffer saline (PBS) solution. The eyes and lenses were imaged under a light microscope (Nikon SMZ1500, Melville, NY). Whole eyes from 6-month-old control and mutant mice exhibiting lenti-corneal stalk were collected and fixed overnight in 4% paraformaldehyde (PFA, Fisher Scientific, Waltham, MA; Catalog number T-353-500) for hematoxylin and eosin (H&E) staining. The samples were then dehydrated with ethanol, and embedded in paraffin for microtome sectioning. Sagittal paraffin sections (5 μm) were stained with H&E according to standard protocol (Manthey et al., 2014a) and visualized using light microscopy (Zeiss Axiophot) and a Nikon digital camera.

Scanning Electron Microscopy

Scanning electron microscopy (SEM) was performed on 1 month old control (*Pax6GFPCre:Caprin2*$^{+/cKO}$) and *Caprin2* $^{cKO/cKO}$ mutant lenses as previously described (Scheiblin et al., 2014). Briefly, whole eyes were dissected without delay from control and mutant mice after euthanization and treated with a fixative containing 0.08M sodium cacodylate pH 7.4, 1.25% glutaraldehyde, 1% paraformaldehyde (Electron Microscopy Sciences, Hatfield, PA) for 3 hours. The lens were dissected from the eye and transferred to fresh cold fixative for 48 hours. The lenses were washed and the lens capsule along with a few layers of fiber cells were removed from one hemisphere of the lens in order to view the fiber cell ultrastructure. The peeled lenses were then dehydrated through an alcohol dilution series and hexamethyldisilazane (HMDS, Sigma, St. Louis, MO) dilution series (diluted in ethanol). Lenses were then subjected to sputter coating with gold/palladium for 2.5 min before imaging with Hitachi S-4700 Field Emission Scanning Electron Microscope (Tokyo, Japan). The analysis was performed on eight biological replicates for both control and mutants.

In Situ Hybridizations

In situ hybridization (ISH) analysis was performed as described in detail (Lachke et al., 2012b). Embryonic head tissue was obtained from E12.5 and E14.5 wild-type ICR mice and fixed overnight in 4% PFA, cryoprotected using 30% sucrose overnight, and embedded in tissue freezing media, OCT (Tissue Tek, Torrance, CA). Frozen sections (coronal) were prepared at 16μm thickness. Primers were designed with either T7 or SP6 promoter sequences upstream of *Caprin2* cDNA-specific region as follows: SP6_Caprin 2-F, 5′ GCTATTTAGGTGACACTATAGATGAAGTCAGCCAAGTCCCA 3′; T7_Caprin 2-R, 5′ TTGTAATACGACTCACTATAGGGCGAAGCTTTTTCTTCTCAGT 3′. These primers were used in PCR to amplify *Caprin2* cDNA region that was subjected to *in vitro* transcription, to in turn generate RNA probes for ISH analysis. Slides hybridized with *Caprin2*-specific antisense probe were viewed and imaged using a light microscope (Zeiss Axiophot) with a Nikon digital camera.

Western Blotting

Lenses were enucleated from control (*Pax6GFPCre:Caprin2*$^{+/cKO}$) and *Caprin2* $^{cKO/cKO}$ mutant mice and dissolved in lysis buffer (50mM Tris HCl pH 8.0, 150 mM NaCl, 0.1% SDS, 1% NP-40 (Tergitol, Sigma-Aldrich, St. Louis, MO; Catalog number NP40S) and 0.8% sodium deoxycholate) on ice. Lysed samples were then spun at 14000 g at 4°C for 30 minutes. The supernatant was collected and protein content was estimated using NanoDrop. Total protein (100 μg) was denatured using 4x lamelli buffer and loaded and run on a 7% SDS-PAGE at 90V for 90 minutes. Protein was then transferred to a PVDF membrane (Fisher Scientific, Waltham, MA; Catalog number PI88518) treated with 100% methanol for 5 minutes at 100V for 1 hour at 4°C. Membrane was blocked with 5% milk in TBST (Tris Buffer Saline with 1% Tween 20) for 1 hour and incubated overnight at 4°C with commercially obtained rabbit antibody against Caprin1 and Caprin2 (diluted 1:200 in 5% milk in TBST) (Proteintech Group, Chicago, IL; Catalog number 15112-1-AP and 20766-1-AP). After overnight incubation, the blot was subjected to three 15 minutes washes with TBST and incubated for an hour at room temperature (RT) with anti-rabbit secondary antibody conjugated with HRP (horse radish peroxidase) (Cell Signaling, Beverly, MA; Catalog number 7074). This was followed by three 15 minutes washes with TBST for 15 minutes before the blot was incubated with the chemiluminescence substrate (GE Healthcare Life Sciences, Pittsburgh, PA; Catalog number RPN2235) and imaged using AlphaImager HP MultiImage II (ProteinSimple, San Jose, CA).

Immunofluorescence

Mouse embryonic head tissue at various stages were embedded in tissue freezing media, OCT (Tissue Tek, Torrance, California) and frozen sections (coronal) were prepared at 16μm thickness as described (Lachke et al., 2011). Sections were fixed with 4% paraformaldehyde in 1x PBS for 20 min at RT followed by two 1x PBS washes and were blocked for 1 hour at RT in 5% goat serum, 1% chicken serum, 0.1% tween in PBS. The sections were then incubated with rabbit primary antibody for Caprin2 (1:50 dilution) and Caprin1 (1:50 dilution) (Proteintech Group, Chicago, IL; Catalog number 20766-1-AP and 15112-1-AP) overnight at 4°C. Slides were washed three times in 1x PBS and incubated for

1 hour at RT with chicken anti-rabbit IgG conjugated to Alexa Fluor 594 secondary antibody (Thermo Fisher Scientific, Waltham, MA; Catalog number B00101) at 1:200 dilution mixed with 1:500 dilution of DAPI (Life Technologies, Carlsbad, CA; Catalog number D21490). Slides were then washed three times with 1x PBS, mounted, and stored at 4°C until imaging using Zeiss LSM 780 confocal configured with Argon/Krypton laser (488 nm and 561 nm excitation) and Helium Neon laser (633 nm excitation) (Carl Zeiss Inc., Gottingen, Germany). Optimal adjustment of brightness/contrast was performed in Adobe Photoshop and applied consistently for all images. For Pax6, Foxe3, Aqp0, N-cad, F-actin, Jag1 and Cryg immunostaining (Manthey et al., 2014a), embryonic head tissue from *Caprin2*$^{cKO/cKO}$ mutant and control (*Pax6GFPCre:Caprin2*$^{+/cKO}$) mice was fixed in 4% PFA for 30 minutes on ice at 4°C and treated with 30% sucrose overnight at 4°C, following which they were embedded in OCT. Frozen sections were prepared at 16 μm thickness. Staining was performed according to specific conditions given in Table 2 and described above for Caprin2 (note: for Pax6 and N-cad staining, 1X TBS (Tris buffer Saline) was used in blocking buffer).

F-actin and Wheat Germ Agglutinin (WGA) Staining and Calculation of Nuclear Fiber Cell Area

Section and whole lens F-actin and WGA staining were performed as reported (Scheiblin et al., 2014). Briefly, embryonic head tissue from *Caprin2* $^{cKO/cKO}$ mutant and control (*Pax6GFPCre:Caprin2*$^{+/cKO}$) mice (Stages E12.5, E14.5, E16.5, P0) was fixed in 4% PFA for 30 minutes on ice at 4°C and treated with 30% sucrose overnight at 4°C, followed by embedding in OCT. Frozen sections were prepared at 16μm thickness. Sections were blocked in blocking buffer (2% BSA in 1x PBS) for 1 hour at RT. They were then incubated in Phalloidin conjugated with Alexa flour 568 and Wheat Germ Agglutinin (Invitrogen, Grand Island, NY) conjugated with Alexa flour 488 (diluted 1:200 in blocking buffer along with 1:500 DAPI) for one hour at RT following which the slides were washed with 1x PBS and mounted. The stained slides were imaged using Confocal 780 (Carl Zeiss Inc.). Lens tissue images at various stages were processed using Photoshop (Adobe, San Jose, CA). Because WGA binds preferentially to the ball and socket junctions in the lens, higher intensity of WGA staining is generally observed in the cortical fiber zone while nuclear fiber zone is stained at reduced intensity (Kistler et al., 1986). The ImageJ (NIH, Bethesda, MD) software was used to calculate the area and fluorescence intensity of the nuclear fiber region (WGA stained at low intensity) and that of the whole lens. Fluorescence intensity of below 30 was described as lower staining and above 30 was described as higher staining. The ratio of the area of the nuclear fiber region to the entire area of the lens was calculated for control and *Caprin2*$^{cKO/cKO}$ mutants in four biological replicates and statistical significance for their difference was estimated using a student *t*-test.

Acknowledgments

We thank Atul Kakrana for helpful discussions and support with mouse lens microarray analysis. *Caprin2*$^{tm2a(EUCOMM)Wtsi}$ allele carrying mice (EMMA ID, EM:05381) were obtained from the European Mouse Mutant Archive (EMMA). This research was supported by NIH/NEI grant R01 EY021505 to D.B. and S.L. S.L. is a Pew Scholar in Biomedical Sciences.

References

Aerbajinai W, Lee YT, Wojda U, Barr VA, Miller JL. Cloning and characterization of a gene expressed during terminal differentiation that encodes a novel inhibitor of growth. J Biol Chem. 2004; 279:1916–1921.10.1074/jbc.M305634200 [PubMed: 14593112]

Agrawal SA, Anand D, Siddam AD, Kakrana A, Dash S, Scheiblin DA, Dang CA, Terrell AM, Waters SM, Singh A, Motohashi H, Yamamoto M, Lachke SA. Compound mouse mutants of bZIP transcription factors Mafg and Mafk reveal a regulatory network of non-crystallin genes associated with cataract. Hum Genet. 2015; 134:717–735.10.1007/s00439-015-1554-5 [PubMed: 25896808]

al-Ghoul KJ, Costello MJ. Fiber cell morphology and cytoplasmic texture in cataractous and normal human lens nuclei. Curr Eye Res. 1996; 15:533–542. [PubMed: 8670754]

Al-Ghoul KJ, Nordgren RK, Kuszak AJ, Freel CD, Costello MJ, Kuszak JR. Structural evidence of human nuclear fiber compaction as a function of ageing and cataractogenesis. Exp Eye Res. 2001; 72:199–214.10.1006/exer.2000.0937 [PubMed: 11180969]

Augusteyn RC. On the growth and internal structure of the human lens. Exp Eye Res. 2010; 90:643–654.10.1016/j.exer.2010.01.013 [PubMed: 20171212]

Bassnett S, Shi Y, Vrensen GFJM. Biological glass: structural determinants of eye lens transparency. Philos Trans R Soc Lond, B, Biol Sci. 2011; 366:1250–1264.10.1098/rstb.2010.0302 [PubMed: 21402584]

Bhandari R, Ferri S, Whittaker B, Liu M, Lazzaro DR. Peters anomaly: review of the literature. Cornea. 2011; 30:939–944.10.1097/ICO.0b013e31820156a9 [PubMed: 21448066]

Cavalheiro GR, Matos-Rodrigues GE, Gomes AL, Rodrigues PMG, Martins RAP. c-Myc regulates cell proliferation during lens development. PLoS ONE. 2014; 9:e87182.10.1371/journal.pone.0087182 [PubMed: 24503550]

Chen Y, Doughman Y, Gu S, Jarrell A, Aota S, Cvekl A, Watanabe M, Dunwoodie SL, Johnson RS, van Heyningen V, Kleinjan DA, Beebe DC, Yang YC. Cited2 is required for the proper formation of the hyaloid vasculature and for lens morphogenesis. Development. 2008; 135:2939–2948.10.1242/dev.021097 [PubMed: 18653562]

Churchill A, Graw J. Clinical and experimental advances in congenital and paediatric cataracts. Philos Trans R Soc Lond, B, Biol Sci. 2011; 366:1234–1249.10.1098/rstb.2010.0227 [PubMed: 21402583]

Costello MJ, Mohamed A, Gilliland KO, Fowler WC, Johnsen S. Ultrastructural analysis of the human lens fiber cell remodeling zone and the initiation of cellular compaction. Exp Eye Res. 2013; 116:411–418.10.1016/j.exer.2013.10.015 [PubMed: 24183661]

Cvekl A, Ashery-Padan R. The cellular and molecular mechanisms of vertebrate lens development. Development. 2014; 141:4432–4447.10.1242/dev.107953 [PubMed: 25406393]

Cvekl A, Duncan MK. Genetic and epigenetic mechanisms of gene regulation during lens development. Prog Retin Eye Res. 2007; 26:555–597.10.1016/j.preteyeres.2007.07.002 [PubMed: 17905638]

Cvekl A, Tamm ER. Anterior eye development and ocular mesenchyme: new insights from mouse models and human diseases. Bioessays. 2004; 26:374–386.10.1002/bies.20009 [PubMed: 15057935]

Donner AL, Lachke SA, Maas RL. Lens induction in vertebrates: variations on a conserved theme of signaling events. Semin Cell Dev Biol. 2006; 17:676–685.10.1016/j.semcdb.2006.10.005 [PubMed: 17164096]

Dubbelman M, Van der Heijde GL, Weeber HA, Vrensen GFJM. Changes in the internal structure of the human crystalline lens with age and accommodation. Vision Res. 2003; 43:2363–2375. [PubMed: 12962993]

Faber SC, Dimanlig P, Makarenkova HP, Shirke S, Ko K, Lang RA. Fgf receptor signaling plays a role in lens induction. Development. 2001; 128:4425–4438. [PubMed: 11714669]

Fudge DS, McCuaig JV, Van Stralen S, Hess JF, Wang H, Mathias RT, FitzGerald PG. Intermediate filaments regulate tissue size and stiffness in the murine lens. Invest Ophthalmol Vis Sci. 2011; 52:3860–3867.10.1167/iovs.10-6231 [PubMed: 21345981]

Garcia CM, Huang J, Madakashira BP, Liu Y, Rajagopal R, Dattilo L, Robinson ML, Beebe DC. The function of FGF signaling in the lens placode. Dev Biol. 2011; 351:176–185.10.1016/j.ydbio.2011.01.001 [PubMed: 21223962]

Hanafusa H, Torii S, Yasunaga T, Nishida E. Sprouty1 and Sprouty2 provide a control mechanism for the Ras/MAPK signalling pathway. Nat Cell Biol. 2002; 4:850–858.10.1038/ncb867 [PubMed: 12402043]

Hay ED. Development of the vertebrate cornea. Int Rev Cytol. 1980; 63:263–322. [PubMed: 395131]

Hendrix RW, Zwaan J. Cell shape regulation and cell cycle in embryonic lens cells. Nature. 1974; 247:145–147. [PubMed: 4810225]

Kasaikina MV, Fomenko DE, Labunskyy VM, Lachke SA, Qiu W, Moncaster JA, Zhang J, Wojnarowicz MW Jr, Natarajan SK, Malinouski M, Schweizer U, Tsuji PA, Carlson BA, Maas RL, Lou MF, Goldstein LE, Hatfield DL, Gladyshev VN. Roles of the 15-kDa selenoprotein (Sep15) in redox homeostasis and cataract development revealed by the analysis of Sep 15 knockout mice. J Biol Chem. 2011; 286:33203–33212.10.1074/jbc.M111.259218 [PubMed: 21768092]

Kistler J, Gilbert K, Brooks HV, Jolly RD, Hopcroft DH, Bullivant S. Membrane interlocking domains in the lens. Invest Ophthalmol Vis Sci. 1986; 27:1527–1534. [PubMed: 3759369]

Kuracha MR, Burgess D, Siefker E, Cooper JT, Licht JD, Robinson ML, Govindarajan V. Spry1 and Spry2 are necessary for lens vesicle separation and corneal differentiation. Invest Ophthalmol Vis Sci. 2011; 52:6887–6897.10.1167/iovs.11-7531 [PubMed: 21743007]

Lachke SA, Alkuraya FS, Kneeland SC, Ohn T, Aboukhalil A, Howell GR, Saadi I, Cavallesco R, Yue Y, Tsai ACH, Nair KS, Cosma MI, Smith RS, Hodges E, Alfadhli SM, Al-Hajeri A, Shamseldin HE, Behbehani A, Hannon GJ, Bulyk ML, Drack AV, Anderson PJ, John SWM, Maas RL. Mutations in the RNA granule component TDRD7 cause cataract and glaucoma. Science. 2011; 331:1571–1576.10.1126/science.1195970 [PubMed: 21436445]

Lachke SA, Higgins AW, Inagaki M, Saadi I, Xi Q, Long M, Quade BJ, Talkowski ME, Gusella JF, Fujimoto A, Robinson ML, Yang Y, Duong QT, Shapira I, Motro B, Miyoshi J, Takai Y, Morton CC, Maas RL. The cell adhesion gene PVRL3 is associated with congenital ocular defects. Hum Genet. 2012a; 131:235–250.10.1007/s00439-011-1064-z [PubMed: 21769484]

Lachke SA, Ho JWK, Kryukov GV, O'Connell DJ, Aboukhalil A, Bulyk ML, Park PJ, Maas RL. iSyTE: integrated Systems Tool for Eye gene discovery. Invest Ophthalmol Vis Sci. 2012b; 53:1617–1627.10.1167/iovs.11-8839 [PubMed: 22323457]

Lachke SA, Maas RL. RNA Granules and Cataract. Expert Rev Ophthalmol. 2011; 6:497–500.10.1586/eop.11.53 [PubMed: 23847690]

Lachke SA, Maas RL. Building the developmental oculome: systems biology in vertebrate eye development and disease. Wiley Interdiscip Rev Syst Biol Med. 2010; 2:305–323.10.1002/wsbm.59 [PubMed: 20836031]

Lang RA, Herman K, Reynolds AB, Hildebrand JD, Plageman TF. p120-catenin-dependent junctional recruitment of Shroom3 is required for apical constriction during lens pit morphogenesis. Development. 2014; 141:3177–3187.10.1242/dev.107433 [PubMed: 25038041]

Le TT, Conley KW, Mead TJ, Rowan S, Yutzey KE, Brown NL. Requirements for Jag1-Rbpj mediated Notch signaling during early mouse lens development. Dev Dyn. 2012; 241:493–504.10.1002/dvdy.23739 [PubMed: 22275127]

Lorén CE, Schrader JW, Ahlgren U, Gunhaga L. FGF signals induce Caprin2 expression in the vertebrate lens. Differentiation. 2009; 77:386–394.10.1016/j.diff.2008.11.003 [PubMed: 19275872]

Lovicu FJ, McAvoy JW. Growth factor regulation of lens development. Dev Biol. 2005; 280:1–14.10.1016/j.ydbio.2005.01.020 [PubMed: 15766743]

Manthey AL, Lachke SA, FitzGerald PG, Mason RW, Scheiblin DA, McDonald JH, Duncan MK. Loss of Sip1 leads to migration defects and retention of ectodermal markers during lens development. Mech Dev. 2014a; 131:86–110.10.1016/j.mod.2013.09.005 [PubMed: 24161570]

Manthey AL, Terrell AM, Lachke SA, Polson SW, Duncan MK. Development of novel filtering criteria to analyze RNA-sequencing data obtained from the murine ocular lens during

embryogenesis. Genomics Data. 2014b; 2:369–374.10.1016/j.gdata.2014.10.015 [PubMed: 25478318]

Michael R, Bron AJ. The ageing lens and cataract: a model of normal and pathological ageing. Philos Trans R Soc Lond, B, Biol Sci. 2011; 366:1278–1292.10.1098/rstb.2010.0300 [PubMed: 21402586]

Okajima K, Robinson LK, Hart MA, Abuelo DN, Cowan LS, Hasegawa T, Maumenee IH, Jabs EW. Ocular anterior chamber dysgenesis in craniosynostosis syndromes with a fibroblast growth factor receptor 2 mutation. Am J Med Genet. 1999; 85:160–170. [PubMed: 10406670]

Ozeki H, Ogura Y, Hirabayashi Y, Shimada S. Suppression of lens stalk cell apoptosis by hyaluronic acid leads to faulty separation of the lens vesicle. Exp Eye Res. 2001; 72:63–70.10.1006/exer.2000.0923 [PubMed: 11133183]

Papoulas O, Monzo KF, Cantin GT, Ruse C, Yates JR, Ryu YH, Sisson JC. dFMRP and Caprin, translational regulators of synaptic plasticity, control the cell cycle at the Drosophila mid-blastula transition. Development. 2010; 137:4201–4209.10.1242/dev.055046 [PubMed: 21068064]

Plageman TF Jr, Chauhan BK, Yang C, Jaudon F, Shang X, Zheng Y, Lou M, Debant A, Hildebrand JD, Lang RA. A Trio-RhoA-Shroom3 pathway is required for apical constriction and epithelial invagination. Development. 2011; 138:5177–5188.10.1242/dev.067868 [PubMed: 22031541]

Plageman TF Jr, Chung MI, Lou M, Smith AN, Hildebrand JD, Wallingford JB, Lang RA. Pax6-dependent Shroom3 expression regulates apical constriction during lens placode invagination. Development. 2010; 137:405–415.10.1242/dev.045369 [PubMed: 20081189]

Pontoriero GF, Deschamps P, Ashery-Padan R, Wong R, Yang Y, Zavadil J, Cvekl A, Sullivan S, Williams T, West-Mays JA. Cell autonomous roles for AP-2alpha in lens vesicle separation and maintenance of the lens epithelial cell phenotype. Dev Dyn. 2008; 237:602–617.10.1002/dvdy.21445 [PubMed: 18224708]

Pontoriero GF, Smith AN, Miller LAD, Radice GL, West-Mays JA, Lang RA. Co-operative roles for E-cadherin and N-cadherin during lens vesicle separation and lens epithelial cell survival. Dev Biol. 2009; 326:403–417.10.1016/j.ydbio.2008.10.011 [PubMed: 18996109]

Reis LM, Semina EV. Genetics of anterior segment dysgenesis disorders. Curr Opin Ophthalmol. 2011; 22:314–324.10.1097/ICU.0b013e328349412b [PubMed: 21730847]

Rowan S, Conley KW, Le TT, Donner AL, Maas RL, Brown NL. Notch signaling regulates growth and differentiation in the mammalian lens. Dev Biol. 2008; 321:111–122.10.1016/j.ydbio.2008.06.002 [PubMed: 18588871]

Rowan S, Siggers T, Lachke SA, Yue Y, Bulyk ML, Maas RL. Precise temporal control of the eye regulatory gene Pax6 via enhancer-binding site affinity. Genes Dev. 2010; 24:980–985.10.1101/gad.1890410 [PubMed: 20413611]

Scheiblin DA, Gao J, Caplan JL, Simirskii VN, Czymmek KJ, Mathias RT, Duncan MK. Beta-1 integrin is important for the structural maintenance and homeostasis of differentiating fiber cells. Int J Biochem Cell Biol. 2014; 50:132–145.10.1016/j.biocel.2014.02.021 [PubMed: 24607497]

Shiels A, Hejtmancik JF. Genetics of human cataract. Clin Genet. 2013; 84:120–127.10.1111/cge.12182 [PubMed: 23647473]

Shiina N, Tokunaga M. RNA granule protein 140 (RNG140), a paralog of RNG105 localized to distinct RNA granules in neuronal dendrites in the adult vertebrate brain. J Biol Chem. 2010; 285:24260–24269.10.1074/jbc.M110.108944 [PubMed: 20516077]

Simirskii VN, Lee RS, Wawrousek EF, Duncan MK. Inbred FVB/N mice are mutant at the cp49/Bfsp2 locus and lack beaded filament proteins in the lens. Invest Ophthalmol Vis Sci. 2006; 47:4931–4934.10.1167/iovs.06-0423 [PubMed: 17065509]

Solomon S, Xu Y, Wang B, David MD, Schubert P, Kennedy D, Schrader JW. Distinct structural features of caprin-1 mediate its interaction with G3BP-1 and its induction of phosphorylation of eukaryotic translation initiation factor 2alpha, entry to cytoplasmic stress granules, and selective interaction with a subset of mRNAs. Mol Cell Biol. 2007; 27:2324–2342.10.1128/MCB.02300-06 [PubMed: 17210633]

Terrell AM, Anand D, Smith SF, Dang CA, Waters SM, Pathania M, Beebe DC, Lachke SA. Molecular characterization of mouse lens epithelial cell lines and their suitability to study RNA

granules and cataract associated genes. Exp Eye Res. 2015; 131:42–55.10.1016/j.exer.2014.12.011 [PubMed: 25530357]

Weh E, Reis LM, Happ HC, Levin AV, Wheeler PG, David KL, Carney E, Angle B, Hauser N, Semina EV. Whole exome sequence analysis of Peters anomaly. Hum Genet. 2014; 133:1497–1511.10.1007/s00439-014-1481-x [PubMed: 25182519]

Wolf L, Harrison W, Huang J, Xie Q, Xiao N, Sun J, Kong L, Lachke SA, Kuracha MR, Govindarajan V, Brindle PK, Ashery-Padan R, Beebe DC, Overbeek PA, Cvekl A. Histone posttranslational modifications and cell fate determination: lens induction requires the lysine acetyltransferases CBP and p300. Nucleic Acids Res. 2013; 41:10199–10214.10.1093/nar/gkt824 [PubMed: 24038357]

Wurm A, Sock E, Fuchshofer R, Wegner M, Tamm ER. Anterior segment dysgenesis in the eyes of mice deficient for the high-mobility-group transcription factor Sox11. Exp Eye Res. 2008; 86:895–907.10.1016/j.exer.2008.03.004 [PubMed: 18423449]

Yan X, Sabrautzki S, Horsch M, Fuchs H, Gailus-Durner V, Beckers J, Hrabě de Angelis M, Graw J. Peroxidasin is essential for eye development in the mouse. Hum Mol Genet. 2014; 23:5597–5614.10.1093/hmg/ddu274 [PubMed: 24895407]

Zhang W, Mulieri PJ, Gaio U, Bae GU, Krauss RS, Kang JS. Ocular abnormalities in mice lacking the immunoglobulin superfamily member Cdo. FEBS J. 2009; 276:5998–6010.10.1111/j.1742-4658.2009.07310.x [PubMed: 19754878]

Zhao J, Kawai K, Wang H, Wu D, Wang M, Yue Z, Zhang J, Liu YH. Loss of Msx2 function down-regulates the FoxE3 expression and results in anterior segment dysgenesis resembling Peters anomaly. Am J Pathol. 2012; 180:2230–2239.10.1016/j.ajpath.2012.02.017 [PubMed: 22503753]

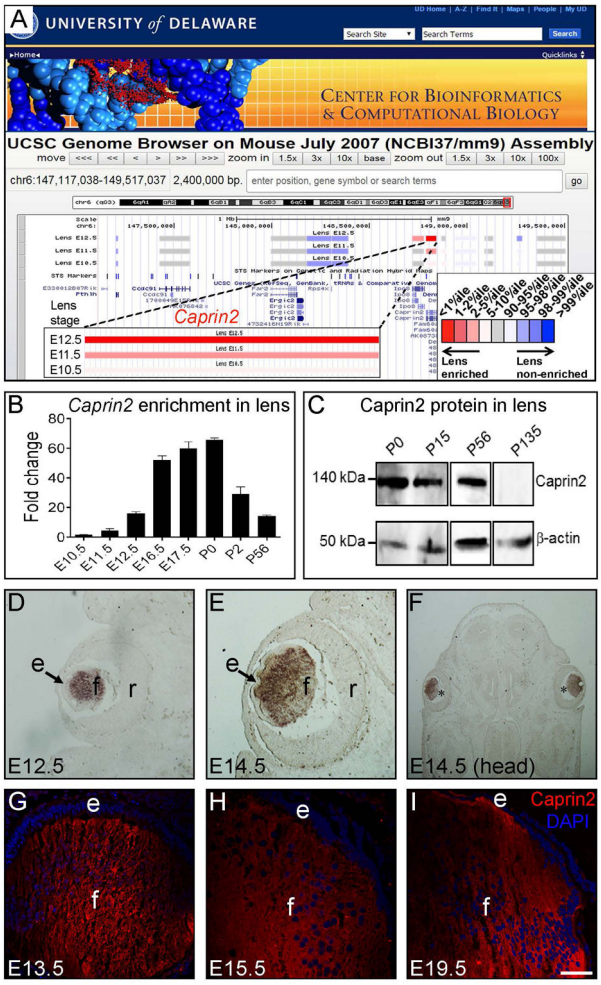

Fig. 1.

Caprin2 exhibits highly enriched expression in mouse lens. (A) *iSyTE* identifies *Caprin2* as a highly lens-enriched gene, as evidenced by intense red color at embryonic stage (E) E12.5. (B) Meta-analysis of mouse lens developmental microarrays ranging from E10.5 to postnatal day (P) 56 indicates highly lens-enriched expression of *Caprin2* compared to embryonic whole body (WB). Relative fold change is the probe binding intensity in lens versus WB. (C) Western blotting demonstrates high Caprin2 protein expression in early postnatal mouse lens (P0, P15) that is progressively reduced (P56), and eventually undetected at P135. (D) RNA probes specific to *Caprin2* cDNA were used for *in situ* hybridization (ISH) on E12.5 and (E) E14.5 mouse head tissue. ISH indicates highly specific expression of *Caprin2* transcripts in fiber cells (f) of the lens, while the lens epithelium (e) or retina (r) exhibits no expression. (F) Low magnification of mouse head tissue section at E14.5 indicates the high specificity and intensity of *Caprin2* expression in the lens (asterisk). (G–I) Immunostaining of mouse head tissue at E13.5, E15.5 and E19.5 demonstrates that Caprin2 protein is highly expressed in fiber cells and not the epithelium (e), validating ISH data. Scale bar in G–I is 70 μm.

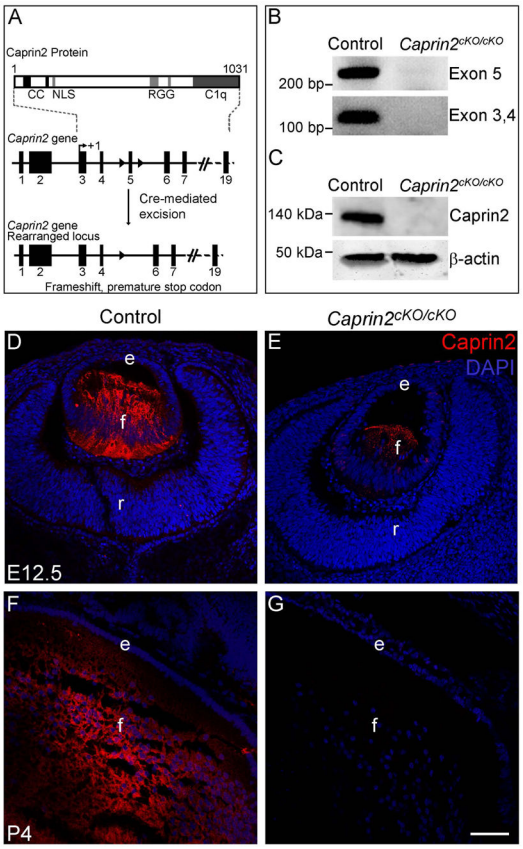

Fig. 2.

Generation of conditional deletion *Caprin2* mice. (A) Structure of the Caprin2 gene locus and depiction of Caprin2 protein. The Caprin2 knockout allele carries exon 5 flanked by *loxP* sites (closed arrowheads). Mouse crosses with a line (*Pax6GFPCre*) that expresses *Cre* recombinase in lens cells beginning at the placode stage results in the excision of *Caprin2* exon 5. This is predicted to generate an abnormal Caprin2 splice form joining exons 4 and 6, in turn leading to a frame-shift and premature stop codon. (B) Reverse transcriptase PCR (RT-PCR) demonstrates the absence of Caprin2 mRNA in homozygous conditional deletion *Caprin2*$^{cKO/cKO}$ mouse mutant lens. (C) Western blotting demonstrates the absence of Caprin2 protein in *Caprin2*$^{cKO/cKO}$ mutant lens at P56. β-actin was used as a loading control. (D, E) Immunostaining analysis at E12.5 exhibits severely reduced but detectable levels of Caprin2 in *Caprin2*$^{cKO/cKO}$ lenses. (F, G) By P4 there is no detectable expression of Caprin2 protein in the mutant lens. Scale bar in D, E is 70 μm. Abbreviation: e, epithelium; f, fiber cells.

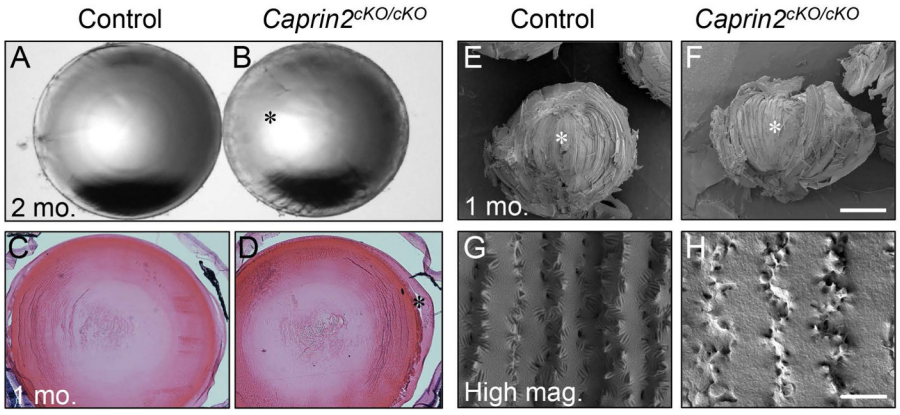

Fig. 3.

Caprin2$^{cKO/cKO}$ mouse mutants exhibit lens defects. (A) Imaging under bright field microscopy revealed subtle differences between control and (B) *Caprin2*$^{cKO/cKO}$ lenses at age 2 months (2 mo.). While a demarcation can be observed in the fiber cell compartment in the controls, it is absent (asterisk) in the mutants. (C–F) Histological analysis demonstrates no obvious defects in *Caprin2*$^{cKO/cKO}$ mutant lenses at age 1 month (1 mo.). (E–H) Scanning electron microscopy of lenses at age 1 month (1 mo.), demonstrates that at comparable depth in the fiber cell compartment, the lens *Caprin2*$^{cKO/cKO}$ mutants exhibit cortical fiber cells instead of nuclear fiber cells, which are observed in control lenses. Asterisks in E and F denote areas observed at high magnification in G, H.

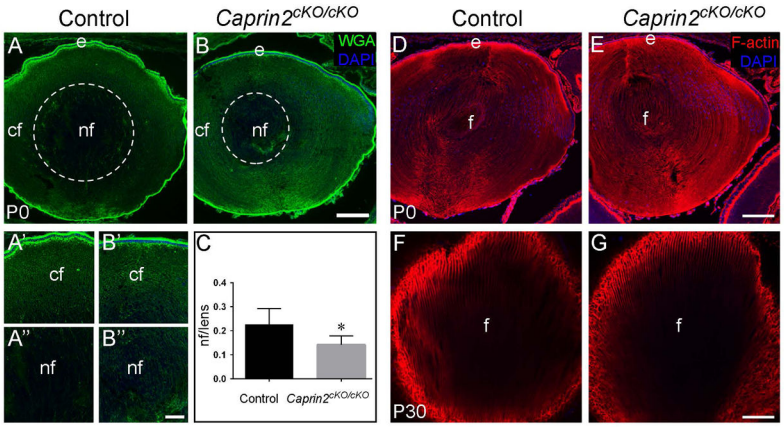

Fig. 4.

Wheat germ agglutinin and Phalloidin staining of *Caprin2*$^{cKO/cKO}$ mutant lens. Wheat germ agglutinin (WGA) staining of (A) control and (B) mutant sections was performed to observe lens cell membranes at stage P0. The area of the nuclear fiber cells with a sharp decrease in WGA staining intensity is indicated by a dotted circle and is reduced in mutants. High magnification images of control (A′, A″) and mutant lenses (B′, B″) show that cortical fibers (cf) exhibit higher WGA staining compared to nuclear fiber (nf). (C) Comparisons between the area of the nf and the area of the lens revealed that mutants have a smaller nf area corroborating the SEM results. (D, E) Section and (F, G) whole lens immunostaining with phalloidin suggests no obvious cytoskeletal defects in the *Caprin2*$^{cKO/cKO}$ lenses. Scale bar for A, B is 140 μm, A′–B″ is 45 μm, for D, E, is 140 μm and F, G is 140 μm. These data demonstrate that although *Caprin2*$^{cKO/cKO}$ lenses do not exhibit lens opacity, they exhibit an overall reduction in the size of the lens nucleus. Abbreviations: cortical fibers (cf), nuclear fibers (nf), epithelium (e), fiber cells (f).

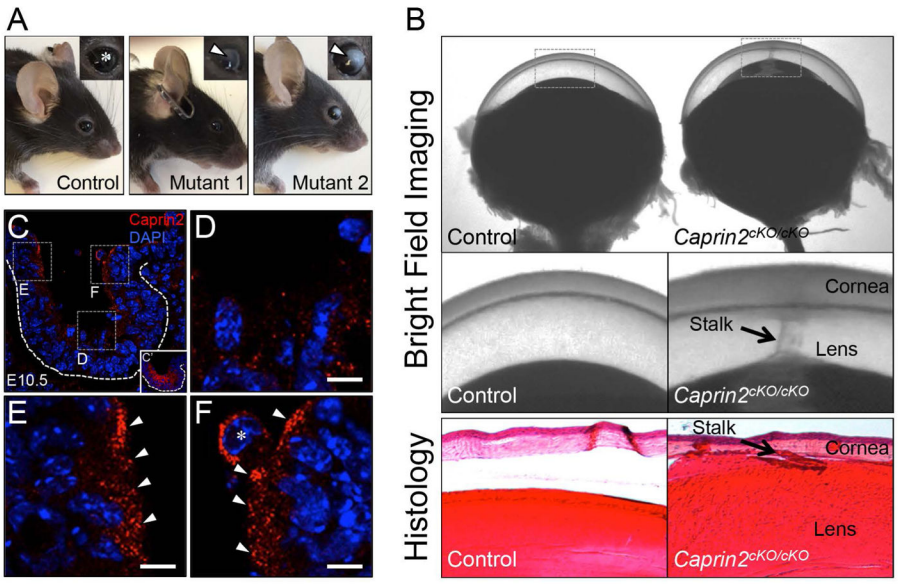

Fig. 5.

Caprin2$^{cKO/cKO}$ mouse mutants exhibit features of Peters anomaly. (A) Images of the eye (inset, high magnification) from control and representative mild (Mutant 1) and severe (Mutant 2) cases of corneal and lens defects. White arrowheads indicate corneal opacity and asterisk denotes reflection of light. (B) Dark field imaging and histology demonstrate that *Caprin2*$^{cKO/cKO}$ mutants exhibit a lenti-corneal stalk similar to Peters anomaly at 8% penetrance (*n*=108 eyes for *Caprin2*$^{cKO/cKO}$ mutants; none exhibit this defect in *Pax6GFPCre:Caprin2*$^{+/cKO}$ controls, *n*=121 eyes). (C) Immunostaining demonstrates the localization of Caprin2 protein in cells of the anterior rim of the lens pit (marked by dotted line) at stage E10.5. (C′) Immunostaining with Jag1 provides better visualization of E10.5 lens pit structure. Broken line boxes in C indicate the regions shown in D, E, and F at high magnification. (D) Caprin2 protein expression is low in the bottom region of the pit. (E, F) However, in cells of the anterior rim region of the lens pit, Caprin2 protein is detected in a granular pattern (white arrowheads). Asterisk indicates a cell that may have originated in the epithelium. Scale bar in C is 28 μm and in D, E, F is 7 μm.

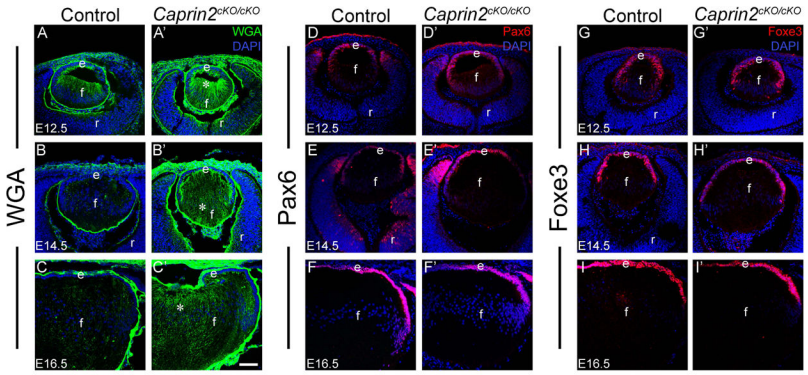

Fig. 6.

Epithelial cell marker and WGA analysis for mouse embryonic *Caprin2*$^{cKO/cKO}$ mutant lens. (A, A′) Wheat germ agglutinin (WGA) staining reveals higher intensity staining (asterisk) in *Caprin2*$^{cKO/cKO}$ mutant lenses compared to control lenses at E12.5, (B, B′) at E14.5, and (C ′, C′) at E16.5. (D, D′) Immunostaining with Pax6-specific antibody reveals no change between control and *Caprin2*$^{cKO/cKO}$ mutant lens at E12.5, (E, E′) at E14.5, and (F′, F′) at E16.5. (G, G′) Immunostaining with Foxe3-specific antibody reveals no change between control (*Pax6GFPCre:Caprin2*$^{+/cKO}$) and *Caprin2*$^{cKO/cKO}$ mutants at E12.5, (H, H′) at E14.5, and (I, I′) at E16.5. Abbreviations: e, epithelium; f, fiber cells; r, retina. Scale bar for all images is 70 μm.

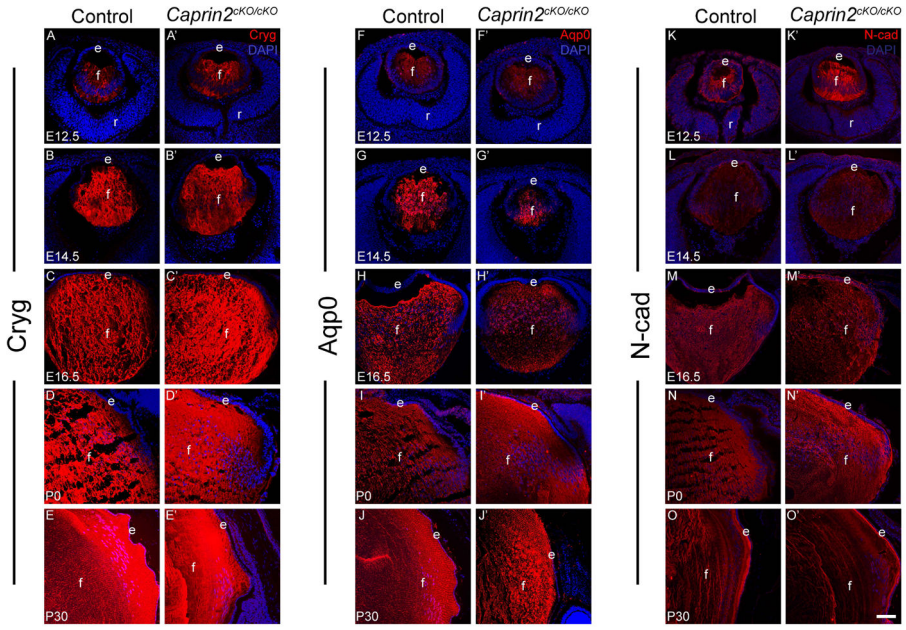

Fig. 7.

Fiber cell marker analysis *Caprin2*$^{cKO/cKO}$ mouse mutant lens. (A, A′) Immunostaining with Crystallin gamma (Cryg) specific antibody reveals no change between control (*Pax6GFPCre:Caprin2*$^{+/cKO}$) and *Caprin2*$^{cKO/cKO}$ mutants at E12.5, (B, B′) at E14.5, (C, C′) at E16.5, (D, D′) at P0 and (E, E′) at P30. (F, F′) Immunostaining with Aquaporin 0 (Aqp0) specific antibody reveals no change between control (*Pax6GFPCre:Caprin2*$^{+/cKO}$) and *Caprin2*$^{cKO/cKO}$ mutants at E12.5, (G, G′) at E14.5, (H, H′) at E16.5, (I, I′) at P0 and (J, J′) at P30. (K, K′) Immunostaining with N-cadherin (N-cad) specific antibody reveals no change between control (*Pax6GFPCre:Caprin2*$^{+/cKO}$) and *Caprin2*$^{cKO/cKO}$ mutants at E12.5, (L, L′) at E14.5, (M′, M′) at E16.5, (N, N′) at P0 and (O, O′) at P30.

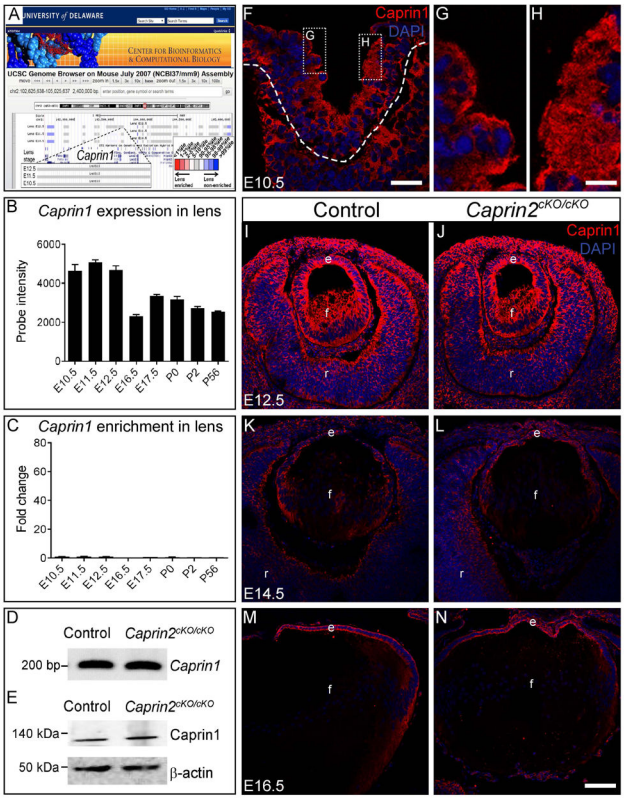

Fig. 8.

Analysis of Caprin1 expression in mouse lens development and *Caprin2*$^{cKO/cKO}$ mutants. (A) *iSyTE* indicates that Caprin1 does not exhibit lens-enriched expression. (B) Analysis of mouse lens microarrays at developmental stages ranging from E10.5 to P56 indicates that *Caprin1* is expressed in the mouse lens. (C) Although expressed in the lens, *Caprin1* is not lens enriched as demonstrated by fold-change comparison of the microarray probe signal binding intensity of *Caprin1* to embryonic whole body (WB) in microarray datasets. (D) RT-PCR analysis of *Caprin1* in control and *Caprin2*$^{cKO/cKO}$ mutant lenses suggest no significant alteration in *Caprin1* mRNA expression. (E) Western blot analysis indicates no significant difference in Caprin1 protein expression in control and *Caprin2*$^{cKO/cKO}$ mutant lenses. (F) Immunostaining of wild type lens demonstrates high Caprin1 protein expression in lens pit cells, including the anterior rim regions (G, H). Broken line box in F indicates the area that is highlighted in G, H. (I, J) Immunostaining with Caprin1-specific antibody reveals no significant difference in control and mutant lenses in E12.5, (K, L) E14.5, and (M, N) E16.5.

Table 1

Frequency of ocular phenotypes in *Caprin2*$^{cKO/cKO}$ mutants

	Pax6GFPCre:Caprin2$^{+/cKO}$	**Caprin2$^{cKO/cKO}$**
Total Number of Lenses	121	108
Normal lenses	118	34 (32%)
* Abnormal lenses	3	65 (60%)
Peters anomaly	0	9 (8%)

* Lenses were recognized as such, based on abnormalities detected near the central region under light microscopy. It should be noted that the reduced lens nucleus defect was observed in 100% of *Caprin2*$^{cKO/cKO}$ mutant lenses when analyzed by scanning electron microscopy (*n*=16) or WGA staining (*n*=8). Therefore, subtle defects may not be detected by light microscopy-based imaging, potentially leading to a higher estimate of false negatives.

Table 2

Antibodies and immunofluorescence conditions

Primary antibody, source and catalog number	Primary antibody conditions	Secondary antibody conditions	Blocking buffer
Foxe3 (Santa Cruz Biotechnology, Dallas, TX, sc-134536)	1:100 in blocking buffer, overnight incubation at 4°C	1:200 Alexa Fluor 594 Chicken anti Rabbit IgG (Thermo Fisher Scientific, Waltham, MA; Catalog number A21442) in blocking buffer	5% chicken serum (Abcam, Cambridge, MA), 0.1% triton X-100 in 1X PBS
Pax6 (Millipore, Billerica, MA, AB2237)	1:200 in blocking buffer, overnight incubation at 4°C	Same as above	5% chicken serum (Abcam, Cambridge, MA), 1% BSA, 0.1% triton X-100 in 1X TBS
N-cad (Abcam, Cambridge, MA ab18203)	1:100 in 1% BSA in PBS	Same as above	1% BSA in PBS
Aqp0 (Millipore, Billerica, MA, AB3071)	1:200 in 2% BSA in PBS	Same as above	2% BSA in PBS
Jag1 (Santa Cruz Biotechnology, Dallas, TX, sc-8303)	1:50 in 2% BSA, 0.1% Triton X-100 in TBS	Same as above	5% goat serum, 0.3% triton X-100 in 1X TsBS
Gamma crystallin (Santa Cruz Biotechnology, Dallas, TX, sc-22415)	1:100 in 1% BSA, 2 % chicken serum, 0.3% TritonX-100 in 1X PBS, 4 hour incubation at RT	1:200 Alexa Fluor 594 Chicken anti goat IgG (Thermo Fisher Scientific, Waltham, MA; Catalog number A-21468) in blocking buffer	5% chicken serum, 0.3% triton X-100 in 1X PBS